Springer

Journal of
Mechanical
Science and
Technology

Journal of Mechanical Science and Technology 23 (2009) 1383~1395

www.springerlink.com/content/1738-494x
DOI 10.1007/s12206-008-1216-9

Transfer matrix for rotor coupler with parallel misalignment †

Chao-Yang Tsai and Shyh-Chin Huang*

Department of Mechanical Engineering National Taiwan University of Science and Technology43, Kee-lung Rd, Sec.4, Taipei, Taiwan 106.R. O. C.

(Manuscript Received December 3, 2007; Revised November 12, 2008; Accepted December 20, 2008)

Abstract

A transfer matrix for shafts coupler with parallel misalignment (offset) was derived. The responses of a rotor system composed of flexible shafts, unbalanced disks, elastic supports and shafts coupler with misalignment were then investigated. Through the derivation, the boundary shears induced by a rotating shaft were first discovered to be coupled in two perpendicular directions. These coupling shears might reduce the first critical speed up to 50% in the free-free case. The studies showed that the shafts coupler altered the rotor's critical speeds and the misalignment played as an external load resulting through the whole driven shaft. The combined effects of disk unbalance and shaft misalignment showed that the misalignment predominated the response in most of the rotation speeds, but the unbalance could become significant at high speed. The whirling orbits before and after the misalignment were illustrated as well, and numerical results showed that the two ends of the misalignment whirled asynchronously as the rotation fell into some regions.

Keywords: Misalignment; Shaft coupler; Transfer matrix method; Unbalance

1. Introduction

Rotors have been extensively used in mechanical engineering, and for over a century the dynamic behavior of rotors has been an interest for study. With the high speed demand of today's machinery, the studies of rotors become more important than ever. Approaches to dynamic analysis of rotor systems may be divided into two main streams: the finite element method (FEM) [1-3] and the transfer matrix method (TMM) [4]. The advantage of TMM is that the matrix dimension does not increase with the number of elements, and instead it is replaced by more matrices multiplications.

As to the existing literature related to TMM, Prohl [5] employed the transfer matrix method for dynamic analysis of rotor systems. Lund and Orcutt [6] established the transfer matrix of a shaft in a continuous fashion rather than discrete but neglected both rotary inertia and gyroscopic effects. Lund [7] considered the internal hysteretic shaft damping and destabilizing aerodynamic forces to calculate the damped natural frequencies of a general flexible rotor supported in fluid-film journal bearing. Chao and Huang [8] introduced the modified transfer matrix extended from Myklestad's transfer matrix in which the Euler beam and rigid disk were the fundamental elements and obtained more precise natural frequencies and shapes. Many researchers [9-11] continuously improved TMM, such as developing oil-film bearing matrix, including rotary inertia, gyroscopic effects of disks. Yet, to the authors' knowledge, none of them included the commonly seen case of shaft misalignment in TMM. The authors hence intend to develop the transfer matrix for a shaft coupler with a parallel offset. Concerning the studies of shaft misalignment, Dewell and Mitchell [12] experimentally studied parallel and angular misalignment of a metallic-disk-type coupling. They used the real time analyzer and verified that the frequencies of all the integer multi-

† This paper was recommended for publication in revised form by Associate Editor Seong-Wook Hong

*Corresponding author. Tel.: +82 2 705 8635, Fax.: +82 2 712 0799
E-mail address: erwin@sogang.ac.kr

ples of rotational speed appeared due to misalignment. They also suggested the 2× and 4× components be used for misalignment diagnosis. Xu and Marangoni adopted a universal joint for misalignment and employed the component mode synthesis to analytically [13] study and experimentally [14] validate the calculations. In their model, the misalignment effects were represented by an additional bending moment of even multiple frequencies of rotation speed. They concluded that the unbalance and misalignment could be characterized by 1× and 2× component, respectively. Sekhar and Prabhu [15] used higher order finite element to study a misaligned rotor-bearing system. In their model, the misalignment effect was replaced by the generated forces and moments on the shaft, and they obtained similar conclusions as [13]. They also concluded that the misalignment had little effect on the critical speeds of a rotor-bearing-coupling system. Lee and Lee [16] employed FEM for a misaligned rotor-bearing system. In their studies, angular, parallel, and combined effects were discussed extensively with shown whirling orbits. In that paper, a shaft coupler was not yet included such that they concluded the whirling orbits tended not to change for parallel misalignment. Al-Hussain and Redmond [17] analytically derived the equations of two Jeffcott rotors with rigid coupling of parallel misalignment. In their conclusions, they did not obtain the 2× component described by the others. Al-Hussain [18] further extended the work to the stability analysis.

The authors here derive the lateral transfer matrix for rotor-bearing system with a flexible coupler and a parallel offset. To form a complete TMM, the transfer matrices for a rotating shaft, an unbalanced disk, an oil-film bearing, and an elastic coupler are briefly described as well. Examples are demonstrated via the developed method. It comes out that the coupler stiffness affects the rotor's critical speeds, but the misalignment plays as an excitation similar to unbalance except it affects through the whole driven shaft. The whirling orbits are investigated as well. The results showed that the two ends of a misalignment may whirl asynchronously as rotation falls into some regions.

2. Transfer matrices

A rotor system containing shafts, disks, bearing supports and a parallel offset coupler is shown schematically in Fig. 1(a). A transfer matrix method for the offset coupler, Fig. 1(b), and for a general rotor consisting of rotating shafts, unbalanced disks, and bearing supports is derived.

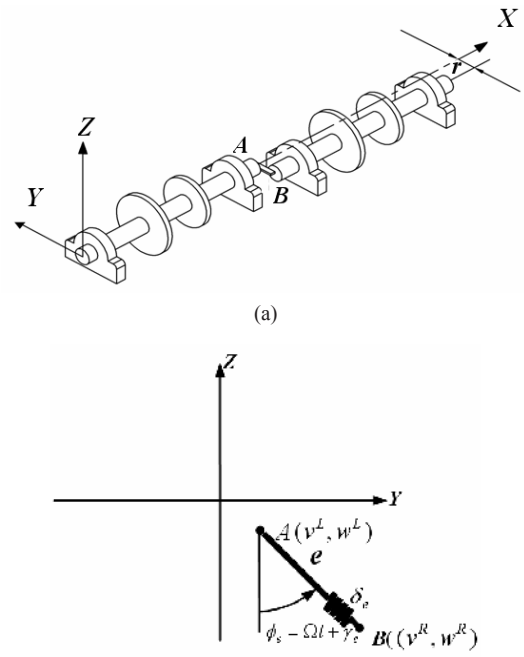

Fig. 1. Schematic diagram of a misaligned rotor: (a) Model of parallel misalignment. (b) Displacement of misalignment.

2.1 Transfer matrix of a rotating shaft

A rotating shaft with coordinates and displacements convention is shown in Fig. 2. Let (v, w) and (θ, ϕ) be the transverse and rotational displacements in Y and Z direction and based on Euler's assumption,

$$\begin{cases} \dfrac{\partial w(X,t)}{\partial X} = -\theta(X,t) \\ \dfrac{\partial v(X,t)}{\partial X} = \phi(X,t) \end{cases} \tag{1}$$

The kinetic energy of a rotating shaft is

$$\begin{aligned} T_s = {} & \frac{1}{2}\int_0^l (\dot{v}^2 + \dot{w}^2)\rho A dX + \frac{1}{2}\int_0^l I_{xx}\Omega^2 \rho dX \\ & + \frac{1}{2}\int_0^l I_{xx}(\dot{\phi}^2 + \Omega^2\theta^2 - 2\Omega\dot{\phi}\theta)\rho dX \\ & + \frac{1}{2}\int_0^l I_{xx}(\dot{\theta}^2 + \Omega^2\phi^2 + 2\Omega\dot{\phi}\theta)\rho dX \end{aligned} \tag{2}$$

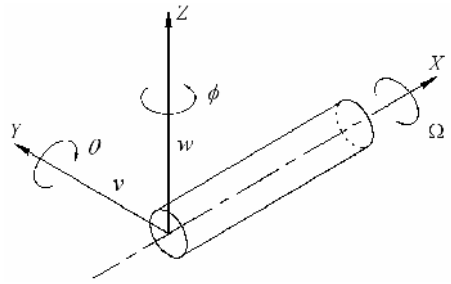

Fig. 2. Coordinate and displacement convention of a rotating shaft.

where ρ, the density of shaft ; l, the length ; A, the cross-section area ; I_{xx}, the polar moment of inertia ; I_{yy}, I_{zz}, the transverse moment of inertia ; $\dot{\theta}$, $\dot{\phi}$, the angular velocity in Y and Z direction, respectively. The subscript "*s*", stands for shaft. Note that the shaft is assumed to be of Rayleigh's type, i.e., including shaft's rotary inertia. The elastic energy due to bending deformation is

$$U_s = \frac{1}{2}\int_0^l \{EI_{zz}[\frac{\partial^2 v}{\partial X^2}]^2 + EI_{yy}[\frac{\partial^2 w}{\partial X^2}]^2\}dX \tag{3}$$

where E is Young's modulus. The work imposed by the boundary forces and moments is

$$\begin{aligned} W_s = \; & (-V_Y^L v^L - V_Z^L w^L - M_Y^L \theta^L - M_Z^L \phi^L) \\ & +(V_Y^R v^R + V_Z^R w^R + M_Y^R \theta^R + M_Z^R \phi^R) \end{aligned} \tag{4}$$

With the extended Hamilton's principle, the equations of motion and the boundary equations are obtained as

$$\begin{cases} EI_{zz} v'''' \\ +\rho[A\ddot{v} - I_{zz}\ddot{v}'' - \Omega(I_{yy} + I_{zz})\dot{w}'' + \Omega^2 I_{yy} v''] = 0 \\ EI_{yy} w'''' \\ +\rho[A\ddot{w} - I_{yy}\ddot{w}'' + \Omega(I_{yy} + I_{zz})\dot{v}'' + \Omega^2 I_{zz} w''] = 0 \end{cases} \tag{5}$$

and

$$\begin{cases} \left\{ \begin{matrix} V_Y + EI_{zz} v''' - \underline{\rho I_{zz}\ddot{v}'} \\ \underline{[-\rho\Omega(I_{yy} + I_{zz})\dot{w}' + \rho\Omega^2 I_{yy} v']} \end{matrix} \right\} \delta v = 0 \\ \left\{ \begin{matrix} V_Z + EI_{yy} w''' - \underline{\rho I_{yy}\ddot{w}'} \\ \underline{[+\rho\Omega(I_{yy} + I_{zz})\dot{v}' + \rho\Omega^2 I_{ZZ} w']} \end{matrix} \right\} \delta w = 0 \\ \{ M_Y + EI_{yy} v'' \} \delta w' = 0 \\ \{ M_Z - EI_{zz} w'' \} \delta v' = 0 \end{cases} \tag{6}$$

Note that Eq. (6) reveals a phenomenon that boundary shears couple with displacements in two perpendicular directions, as underlined, due to the occurrence of rotation, unlike a non-rotating shaft. The coupling terms could be significant at very high rotational speed as to be shown. The solutions to Eq. (5) are of the forms:

$$\begin{cases} \begin{cases} v(X,t) = v(x)\ \cos\omega t \\ \phi(X,t) = \phi(x)\ \cos\omega t \\ M_Z(X,t) = M_Z(x)\ \cos\omega t \\ V_Y(X,t) = V_Y(x)\ \cos\omega t \end{cases} \\ \begin{cases} v(X,t) = v(x)\ \sin\omega t \\ \phi(X,t) = \phi(x)\ \sin\omega t \\ M_Z(X,t) = M_Z(x)\sin\omega t \\ V_Y(X,t) = V_Y(x)\sin\omega t \end{cases} \end{cases} \tag{7}$$

or

$$\begin{cases} \begin{cases} v(X,t) = v(x)\ \sin\omega t \\ \phi(X,t) = \phi(x)\ \sin\omega t \\ M_Z(X,t) = M_Z(x)\ \sin\omega t \\ V_Y(X,t) = V_Y(x)\ \sin\omega t \end{cases} \\ \begin{cases} v(X,t) = v(x)\ \cos\omega t \\ \phi(X,t) = \phi(x)\ \cos\omega t \\ M_Z(X,t) = M_Z(x)\cos\omega t \\ V_Y(X,t) = V_Y(x)\cos\omega t \end{cases} \end{cases} \tag{8}$$

Substitute Eq. (7) or (8) into Eq. (5) and separate the time and space variables. An eigenvalue problem is yielded as

$$\begin{cases} v'''' + a_1 v'' - a_2 w'' - a_3 v = 0 \\ w'''' + b_1 w'' - b_2 v'' - b_3 w = 0 \end{cases} \tag{9}$$

with the boundary conditions,

$$\begin{cases} V_Y / EI_{zz} + v''' + a_1 v' - a_2 w' = 0 \quad or \quad \delta v = 0 \\ V_Z / EI_{yy} + w''' - b_1 w' - b_2 w' = 0 \quad or \quad \delta w = 0 \\ M_Y + EI_{yy} v'' = 0 \qquad or \qquad \delta w' = 0 \\ M_Z - EI_{zz} w'' = 0 \qquad or \qquad \delta v' = 0 \end{cases} \tag{10}$$

where

$$\begin{cases} a_1 = \dfrac{\rho(\omega^2 I_{zz} + \Omega^2 I_{yy})}{EI_{zz}} \\ a_2 = \dfrac{\rho\Omega\omega(I_{yy} + I_{zz})}{EI_{zz}} \\ a_3 = \dfrac{\rho A\omega^2}{EI_{zz}} \end{cases} \quad \begin{cases} b_1 = \dfrac{\rho(\omega^2 I_{yy} + \Omega^2 I_{zz})}{EI_{yy}} \\ b_2 = \dfrac{\rho\Omega\omega(I_{yy} + I_{zz})}{EI_{yy}} \\ b_3 = \dfrac{\rho A\omega^2}{EI_{yy}} \end{cases} \tag{11}$$

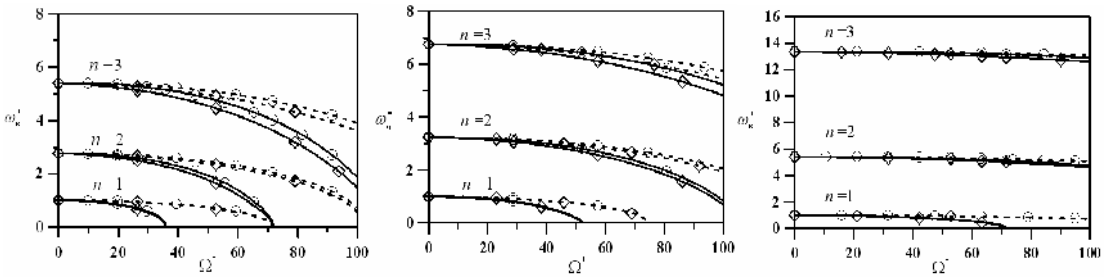

Fig. 3. Natural frequencies of a rotating shaft with different boundary. (a) free-free. (b) simple-free. (c) sliding-free.

Coupled ○ Forward modes — — — Uncoupled ◇ Backward modes

Eqs. (9, 10) present a standard eigenvalue problem with the eigenvalue (ω^2) appearing in both the interior and the boundary equations. The general solutions to Eq. (9) are of the following forms:

$$\begin{cases} v(x) = c_1 \cosh \beta_1 x \\ \qquad + c_2 \sinh \beta_1 x + c_3 \cos \beta_2 x + c_4 \sin \beta_2 x \\ w(x) = c_5 \cosh \beta_3 x \\ \qquad + c_6 \sinh \beta_3 x + c_7 \cos \beta_4 x + c_8 \sin \beta_4 x \end{cases} \tag{12}$$

with

$$\begin{aligned} \beta_1 &= \sqrt{\frac{\sqrt{(a_1 - b_2)^2 + 4a_3} - (a_1 - b_2)}{2}} \\ \beta_2 &= \sqrt{\frac{\sqrt{(a_1 - b_2)^2 + 4a_3} + (a_1 - b_2)}{2}} \\ \beta_3 &= \sqrt{\frac{\sqrt{(b_1 - a_2)^2 + 4b_3} - (b_1 - a_2)}{2}} \\ \beta_4 &= \sqrt{\frac{\sqrt{(b_1 - a_2) + 4b_3} + (b_1 - a_2)}{2}} \end{aligned} \tag{13}$$

in which $c_1, c_2, \ldots, c_8$ are unknown coefficients to be determined from the boundary equations.

Fig. 3 illustrates how the coupling shears affect the shaft's natural frequencies with rotational speed, where $\omega_n^* = \omega_n / \omega_0$, $\Omega^* = \Omega / \omega_0$ and ω_n is the rotating shaft's nth natural frequency and ω_0 is the shaft's first flexural natural frequency at $\Omega = 0$. The free-free case exhibits very significant coupling effects. In these figures, both forward and backward frequencies are illustrated. Note that the coupled solutions have lower natural frequencies. That means the real shaft's critical speeds may be lower than those without coupling shears being taken into account, e.g., around 50% for free-free case and 30% difference for pin-free case.

For rotor dynamics, whirl speed (ω) is equal to the rotational speed (Ω) as far as the steady response is concerned. Eqs. (7, 8) are hence rewritten as

$$\begin{cases} v(X,t) = v_c(x)\cos\Omega t + v_s(x)\sin\Omega t \\ \phi(X,t) = \phi_c(x)\cos\Omega t + \phi_s(x)\sin\Omega t \\ M_Z(X,t) = M_{Zc}(x)\cos\Omega t + M_{Zs}(x)\sin\Omega t \\ V_Y(X,t) = V_{Yc}(x)\cos\Omega t + V_{Ys}(x)\sin\Omega t \\ w(X,t) = w_s(x)\sin\Omega t + w_c(x)\cos\Omega t \\ \theta(X,t) = \theta_s(x)\sin\Omega t + \theta_c(x)\cos\Omega t \\ M_Y(X,t) = M_{Ys}(x)\sin\Omega t + M_{Yc}(x)\cos\Omega t \\ V_Z(X,t) = V_{Zs}(x)\sin\Omega t + V_{Zc}(x)\cos\Omega t \end{cases} \tag{14}$$

The state vector of a rotating Rayleigh shaft can be represented as

$$\{S\} = \{\{S_1\} \ \{S_2\} \ 1\}^T \tag{15}$$

where $\{S\}$ is a 17 × 1 state vector

$$\begin{cases} \{S_1\} = \{v_c \ \ \phi_c \ \ M_{Zc} \ \ V_{Yc} \ \ w_s \ \ \theta_s \ \ M_{Ys} \ \ V_{Zs}\} \\ \{S_2\} = \{v_s \ \ \phi_s \ \ M_{Zs} \ \ V_{Ys} \ \ w_c \ \ \theta_c \ \ M_{Yc} \ \ V_{Zc}\} \end{cases} \tag{16}$$

The transfer matrix of a rotating shaft becomes

$$[T_s]_{17\times17} = \begin{bmatrix} [T_s]_{8\times8} & [0]_{8\times8} & \{0\}_{8\times1} \\ [0]_{8\times8} & [\hat{T}_s]_{8\times8} & \{0\}_{8\times1} \\ \{0\}_{1\times8} & \{0\}_{1\times8} & 1 \end{bmatrix} \tag{17}$$

where $[T_s]$ is the transfer matrix of state vector $\{S_1\}^R$ and $\{S_1\}^L$; $[\hat{T}_s]$ is that of state vector

$\{S_2\}^R$ and $\{S_2\}^L$. Superscripts R and L represent the right and left states, respectively. The elements of $[T_s]$ and $[\hat{T}_s]$ are given in the Appendix.

2.2 Transfer matrix of an unbalanced disk

Each unbalanced disk is equivalent to an unbalanced mass m_e with an eccentricity r_e and an unbalanced angle a_e. The kinetic energy of the unbalanced disk is

$$\begin{aligned} T_d &= \frac{1}{2}m(\dot{v}^2+\dot{w}^2) \\ &+\frac{1}{2}I_z(\dot{\phi}^2+\Omega^2\theta^2-2\Omega\dot{\phi}\theta) \\ &+\frac{1}{2}I_x\Omega^2+\frac{1}{2}I_y(\dot{\theta}^2+\Omega^2\phi^2+2\Omega\dot{\theta}\phi) \\ &+\frac{1}{2}m_e[\dot{v}^2+\dot{w}^2+r_e^2\Omega^2-2r_e\Omega\dot{v}\sin(\Omega t+a_e)] \\ &+\frac{1}{2}m_e[2r_e\Omega\dot{w}\cos(\Omega t+a_e)] \end{aligned} \tag{18}$$

where $\dot{v}$, $\dot{w}$ are the angular velocity of disk in Y and Z direction, respectively. Because the disk is considered to be rigid here, therefore,

$$U_d = 0 \tag{19}$$

The work imposed by the boundary forces and moments is

$$\begin{aligned} W_d &= (V_Y^R - V_Y^L)v + (V_Z^R - V_Z^L)w \\ &+ (M_Y^R - M_Y^L)\theta + (M_Z^R - M_Z^L)\phi \end{aligned} \tag{20}$$

Equations of motion of the unbalanced disk are

$$\begin{cases} M_Y^R = M_Y^L + I_y\ddot{\theta} + I_x\Omega\dot{\phi} \\ M_Z^R = M_Z^L + I_z\ddot{\phi} - I_x\Omega\dot{\theta} \end{cases} \tag{21}$$

$$\begin{cases} V_Y^R = V_Y^L + (m+m_e)\dot{v} - m_e r_e\Omega^2\cos\alpha_e\cos\Omega t \\ \qquad + m_e r_e\Omega^2\sin\alpha_e\sin\Omega t \\ V_Z^R = V_Z^L + (m+m_e)\dot{w} - m_e r_e\Omega^2\sin\alpha_e\cos\Omega t \\ \qquad - m_e r_e\Omega^2\cos\alpha_e\sin\Omega t \end{cases} \tag{22}$$

Substituting Eq. (14) into Eqs. (21,22) and separating the time and space variables, the transfer matrix of an unbalanced disk becomes

$$[T_{ud}]_{17\times17} = \begin{bmatrix} [T_d^*]_{8\times8} & [0]_{8\times8} & \{u_1\}_{8\times1} \\ [0]_{8\times8} & [T_d^{**}]_{8\times8} & \{u_2\}_{8\times1} \\ \{0\}_{1\times8} & \{0\}_{1\times8} & 1 \end{bmatrix} \tag{23}$$

where

$$\begin{cases} \{u_1\} = \begin{Bmatrix} 0 & 0 & 0 & -m_e r_e\Omega^2\cos\alpha_e \\ 0 & 0 & 0 & -m_e r_e\Omega^2\cos\alpha_e \end{Bmatrix}^T \\ \{u_2\} = \begin{Bmatrix} 0 & 0 & 0 & -m_e r_e\Omega^2\sin\alpha_e \\ 0 & 0 & 0 & -m_e r_e\Omega^2\sin\alpha_e \end{Bmatrix}^T \end{cases} \tag{24}$$

The elements of $[T_d]$ are given in the Appendix. $[T_d^*]$, $[T_d^{**}]$ are the same as $[T_d]$ except the following elements:

$$\begin{cases} T_{d3,6}^{**} = T_{d7,2}^{**} = -T_{d3,6}^{*} = -T_{d7,2}^{*} = I_x\Omega^2 \\ T_{d4,1}^{**} = T_{d8,5}^{**} = T_{d4,1}^{*} = T_{d8,5}^{*} = -(m+m_e)\Omega^2 \end{cases} \tag{25}$$

2.3 Transfer matrix of an oil-filmed bearing

Bearing support is an essential component in rotor systems. The springs and damping effects of a bearing have significant influence on dynamic characteristics. Assume an oil-filmed bearing to be of springs and damping including cross-coupling terms. One can obtain the governing equation of oil-filmed bearing [19]:

$$\begin{cases} M_Z^R = M_Z^L + k_{\phi\phi}\phi + k_{\phi\theta}\theta + C_{\phi\phi}\dot{\phi} + C_{\phi\theta}\dot{\theta} \\ M_Y^R = M_Y^L + k_{\theta\theta}\theta + k_{\theta\phi}\phi + C_{\theta\theta}\dot{\theta} + C_{\theta\phi}\dot{\phi} \end{cases} \tag{26}$$

$$\begin{cases} V_Y^R = V_Y^L + k_{yy}v + k_{yz}w + C_{yy}\dot{v} + C_{yz}\dot{w} \\ V_Z^R = V_Z^L + k_{zz}w + k_{zy}v + C_{zz}\dot{w} + C_{zy}\dot{v} \end{cases} \tag{27}$$

Similarly, substituting Eq. (14) into Eqs. (26, 27) and separating the time and space variables, the transfer matrix of an oil-filmed bearing is obtained as

$$[T_b]_{17\times17} = \begin{bmatrix} [T_{b1}]_{8\times8} & [T_{b2}]_{8\times8} & \{0\}_{8\times1} \\ [T_{b3}]_{8\times8} & [T_{b4}]_{8\times8} & \{0\}_{8\times1} \\ \{0\}_{1\times8} & \{0\}_{1\times8} & 1 \end{bmatrix} \tag{28}$$

where $[T_b]$ entries are shown in the Appendix .

2.4 Transfer matrix of a parallel misalignment

Two shafts connected through a coupler are frequently seen in a long rotor system. A coupler provides some elastic connection between shafts. Yet, the coupler may also cause misalignment to some extent if it is not well adjusted. There can be identi-

fied two types of shaft misalignment: parallel offset and angular offset. In the present studies, a coupler is modeled as a linear spring combined with a bending spring. Between two shaft axes, there is a parallel offset as shown in Fig. 1(a). We here intend to derive the corresponding transfer matrix of that parallel offset. The initial (static) offset prior to rotation is assumed to be e and it will displace in the Y - Z plane during rotation due to coupler flexibility, as illustrated in Fig. 1(b). According to the equilibrium relations, we derive the misalignment transfer matrix in the following:

$$v^R = v^L + \frac{V_y}{K_L} + e \cdot \sin(\Omega t + \gamma_e) \tag{29}$$

$$\phi^R = \phi^L - \frac{1}{K_B} M_z^L \tag{30}$$

$$w^R = w^L - \frac{V_z}{K_L} - e \cdot \cos(\Omega t + \gamma_e) \tag{31}$$

$$\theta^R = \theta^L - \frac{1}{K_B} \cdot M_y^L \tag{32}$$

The moments, shear forces are continuous, i.e., $M^R = M^L$, $V^R = V^L$. K_L and K_B are linear and bending stiffness of the coupler. $\phi_e = \Omega t + \gamma_e$, γ_e is a phase angle relative to the rotor's reference. Note that the torsional vibration is not considered so that $\phi_e = \Omega t + \gamma_e$ is retained all the time. $r = e + \delta_e$ is dynamic offset, δ_e is the deflection of linear spring. Substituting Eq. (14) into Eqs. (29-32), the transfer matrix of misalignment yields to be

$$\{S\}^R = [M]\{S\}^L + \{C\} \tag{33}$$

where

$$[M] = \begin{bmatrix} [M_1]_{8\times8} & [M_2]_{8\times8} & \{0\}_{8\times1} \\ [M_3]_{8\times8} & [M_4]_{8\times8} & \{0\}_{8\times1} \\ \{0\}_{1\times8} & \{0\}_{1\times8} & 1 \end{bmatrix} \tag{34}$$

is the defined coupler transfer matrix, and

$$\{C\}_{17\times1} = \{\{C_1\}\ \{C_2\}\ 1\}^T \tag{35}$$

the defined misalignment vector with

$$\begin{cases} \{C_1\} = \{\ e\sin\gamma_e\ \ 0\ \ 0\ \ 0\ \ e\sin\gamma_e\ \ 0\ \ 0\ \ 0\} \\ \{C_2\} = \{\ e\cos\gamma_e\ \ 0\ \ 0\ \ 0\ -e\cos\gamma_e\ \ 0\ \ 0\ \ 0\} \end{cases} \tag{36}$$

$[M]$ entries are shown in the Appendix .

Eq. (33) is for the first time derived, the transfer matrix of a coupler with parallel misalignment. $[M]$ similar to the others, is the transfer matrix that links the left and right states of a coupler, and $\{C\}$ is the misalignment vector that is likened to an exciting force in an unbalanced rotor. It will be seen that after multiplication to its right matrices, all components to the right of the misalignment contribute to the excitation. That means the driven parts behind the misalignment act as a whole in the excitation to the rotor. If there is no misalignment (e=0), $\{C\}$ vanishes and Eq. (33) simply represents a transfer relation of a coupler.

2.5 Total transfer matrix and response analysis

Assume a typical misaligned rotor system as shown in Fig. 4, where there is a misaligned coupler between the k^{th} and k+1$^{\text{th}}$ elements. The overall transfer matrix containing disk unbalance and shaft misalignment is derived to be

$$\{S\}_n^R = [T^u]\{S\}_1^L + [T^m]\{C\} \tag{37}$$

where $\{S\}_1^L$ represents the left state of unit 1, $\{S\}_n^R$ is the right state of unit n, and

$$\begin{cases} [T^u] = T]_n[T]_{n-1} \cdots [T]_{k+1}[M][T]_k[T]_{k-1} \cdots [T]_2[T]_1 \\ [T^m] = [T]_n\ [T]_{n-1}[T]_{n-2} \cdots\cdots [T]_{k+1} \end{cases} \tag{38}$$

Note that $[T]_i$ denotes the i^{th} element transfer matrix, which could be shaft, bearing, or disk. $[T^u]$ is the overall transfer matrix yielded by the multiplication of all transfer matrices and $[T^m]$ is the multiplication of the transfer matrices to the right of misalignment, i.e., from k+1 to n.

Substituting the boundary conditions into Eq. (37), a 9 × 9 matrix will yield

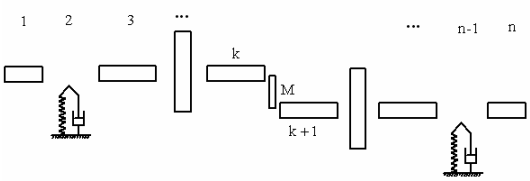

Fig. 4. Schematic diagram of a misaligned rotor in transfer matrix method.

$$\begin{Bmatrix} \{0\}_{8\times1} \\ 1 \end{Bmatrix} = \begin{bmatrix} [T^u]'_{8\times8} & \{u\}_{8\times1} \\ \{0\}_{1\times8} & 1 \end{bmatrix} \begin{Bmatrix} \{S'\}^L_{8\times1} \\ 1 \end{Bmatrix} + \begin{Bmatrix} [m]_{8\times4} \\ \{0\}_{1\times4} \end{Bmatrix} \cdot \{C'\}_{4\times1} \quad (39)$$

with the condensed misalignment vector

$$\{C'\}_{4\times1} = \{-e\sin\gamma_e, -e\sin\gamma_e, -e\cos\gamma_e, e\cos\gamma_e\}^T \quad (40)$$

where elements of $[T^u]'$, $\{u\}$ and $[m]$ are the degeneration of $[T^u]$ and $[T^m]$ matrices. The entries of the above matrices depend on different boundary conditions, as summarized in Table 1. Furthermore, simplifying the above equation and rearranging, one can write it as

$$\begin{bmatrix} [T^u]'_{8\times8} & \{u\}_{8\times1} \\ \{0\}_{1\times8} & 1 \end{bmatrix} \begin{Bmatrix} \{S'\}^L_{8\times1} \\ 1 \end{Bmatrix} = \begin{Bmatrix} -[m]_{8\times4} \cdot \{C'\}_{4\times1} \\ 1 \end{Bmatrix} \quad (41)$$

or

$$[T^u]'_{8\times8} \times \{S'\}^L_{8\times1} = -\{u\}_{8\times1} - [m]_{8\times4} \cdot \{C'\}_{4\times1} \quad (42)$$

There are two effects in Eq. (42). On the right side, the first term is the unbalanced excitation and the second term is the misalignment excitation. Provided the misalignment is zero (e = 0), Eq. (42) yields an unbalanced response analysis. If the coupler stiffness K_B and K_L approach infinity, [M] matrix becomes an identity matrix, representing a rigid coupler.

Table 1. Entries of $[T^u]'$, $\{u\}$, and $[m]$.

left b.c	columns of $[T^u]'$ from $[T^u]$	right b.c	rows of $[T^u]'$
Free	1,2,5,6,9,10,13,14	Free	3,4,7,8,11,12,15,16
Simple	2,4,6,8,10,12,14,16	Simple	1,3,5,7,9,11,13,15
Clamped	3,4,7,8,11,12,15,16	Clamped	1,2,5,6,9,10,13,14
Sliding	1,3,5,7,9,11,13,15	Sliding	2,4,6,8,10,12,14,16
left b.c	columns of $\{u\}$ from $[T^u]$ (unbalance)	right b.c	rows of $\{u\}$
Free	17	Free	3,4,7,8,11,12,15,16
Simple	17	Simple	1,3,5,7,9,11,13,15
Clamped	17	Clamped	1,2,5,6,9,10,13,14
Sliding	17	Sliding	2,4,6,8,10,12,14,16
left b.c	columns of $\{m\}$ from $[T^m]$ (misalignment)	right b.c	rows of $[m]$
Free	1,5,9,13	Free	3,4,7,8,11,12,15,16
Simple	1,5,9,13	Simple	1,3,5,7,9,11,13,15
Clamped	1,5,9,13	Clamped	1,2,5,6,9,10,13,14
Sliding	1,5,9,13	Sliding	2,4,6,8,10,12,14,16

3. Numerical results

In the following, examples that demonstrate the influence of coupler and misalignment via the developed transfer matrix method are illustrated. The rotor system, as illustrated in Fig. 5, consists of three bearings, four rigid disks, and seven-section flexible shaft. The flexibility modulus is,E=20.69 $\times 10^{10} N/m^2$, densityρ=8193.0kg/m^3, and the three bearings are of the same constants in Y and Z direction (K_{yy}= K_{zz}=1.75 $\times 10^8 N$-m). Detailed dimensions of disks and shafts are shown in Table 2.

To begin with, we first look into the influence of the coupler stiffness on the rotor's forward critical speeds. Fig. 6 shows the first three critical speeds as functions of the coupler stiffness K_L. The results show

Table 2. Material and geometric parameters of illustrated example.

Disk No.		Polar Inertia	Diameteral Inertia
1	11.38	19.53	9.82
5	7.88	16.7	8.35
7	7.70	17.61	8.80
12	21.70	44.48	22.24
Shaft No.	Length (cm)	Radius (cm)	
2	8.89	Outer Radius = 2.950cm Inner Radius = 1.680cm	
4	1.6		
6	9.68		
8	7.52		
10	5.60		
11	5.60		
13	7.52		

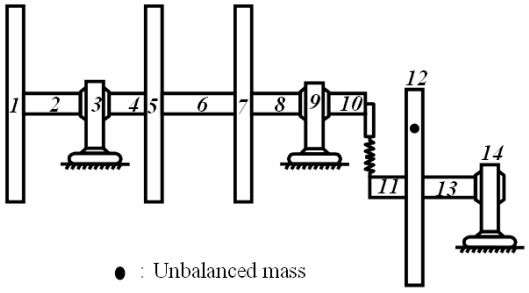

Fig. 5. Example of a misaligned rotor.

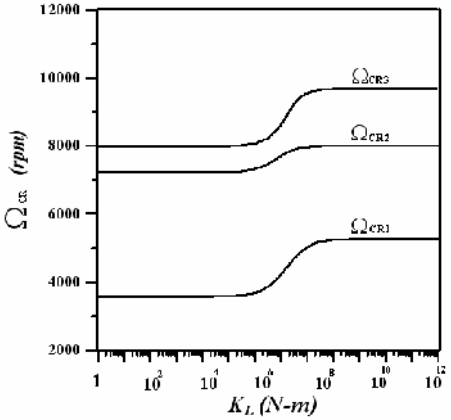

Fig. 6. Influence of coupler stiffness on forward critical speeds.

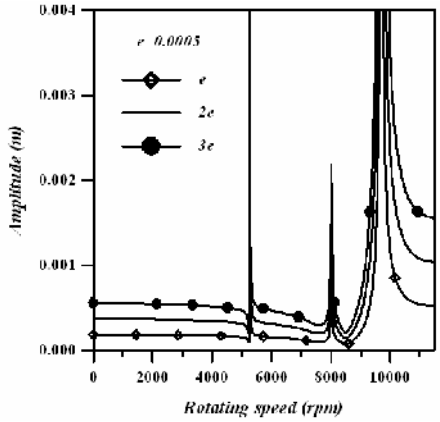

Fig. 7. FRF due to misalignment.

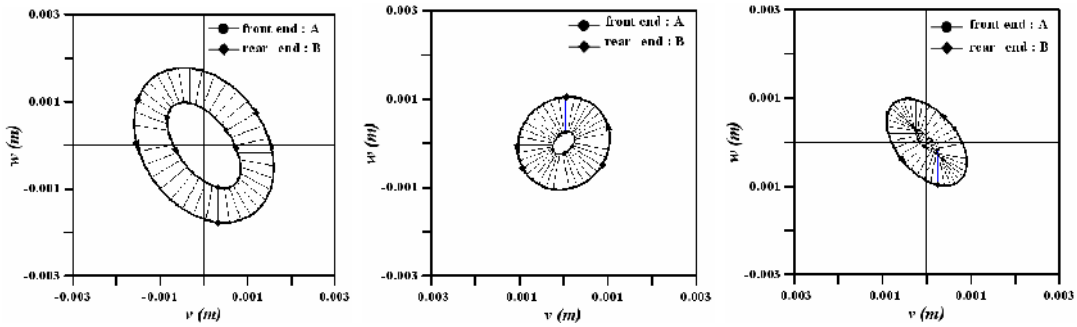

(a) $\Omega < \Omega_{cr1}$ (b) $\Omega_{cr1} < \Omega < \Omega_{cr2}$ (c) $\Omega_{cr2} < \Omega < \Omega_{cr3}$

Fig. 8. Whirling orbits at different rotational speed for K_L in rigid area.

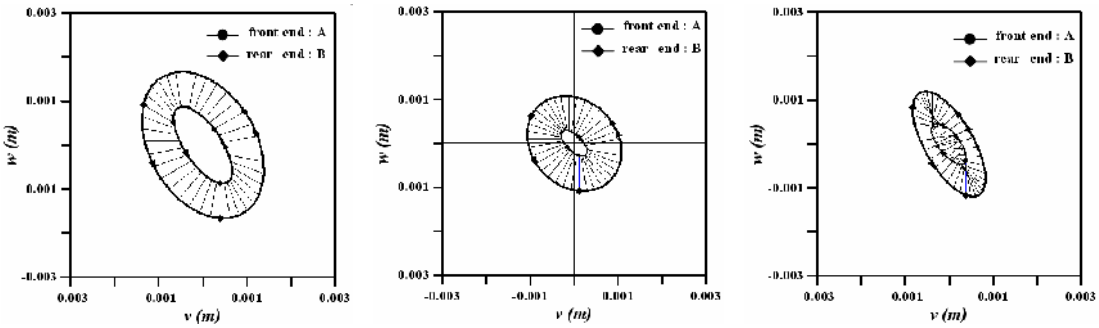

(a) $\Omega < \Omega_{cr1}$ (b) $\Omega_{cr1} < \Omega < \Omega_{cr2}$ (c) $\Omega_{cr2} < \Omega < \Omega_{cr3}$

Fig. 9. Whirling orbits at different rotational speed for K_L in sensitive area.

that as K_L is between 0 and $0.25 \times 10^7 N\text{-}m$ (soft area) and the critical speeds are hardlychanged with K_L. It corresponds to a very soft coupler case so that the critical speeds are basically dominated by the driving part of the rotor. Similarly, as K_L exceeds $0.376 \times 10^{11} N\text{-}m$ (rigid area), it corre sponds to an almost rigid coupler and the combined rotor dominates the critical speeds. When K_L falls in the region of $0.25 \times 10^7 N\text{-}m < K_L < 0.376 \times 10^{11} N\text{-}m$ (sensitive area), the critical speeds are very sensitive to K_L such that a slight change of K_L may result in significant change of critical speeds.

Fig. 7 shows the FRF of the rotor with three different offset values. Cross-referencing Fig. 7 and Eqs.

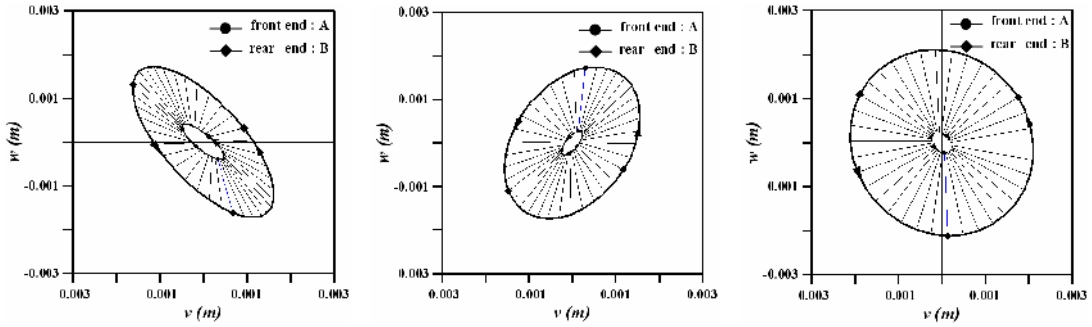

(a) $\Omega < \Omega_{cr1}$ (b) $\Omega_{cr1} < \Omega < \Omega_{cr2}$ (c) $\Omega_{cr2} < \Omega < \Omega_{cr3}$

Fig. 10. Whirling orbits at different rotational speed for K_L in soft area.

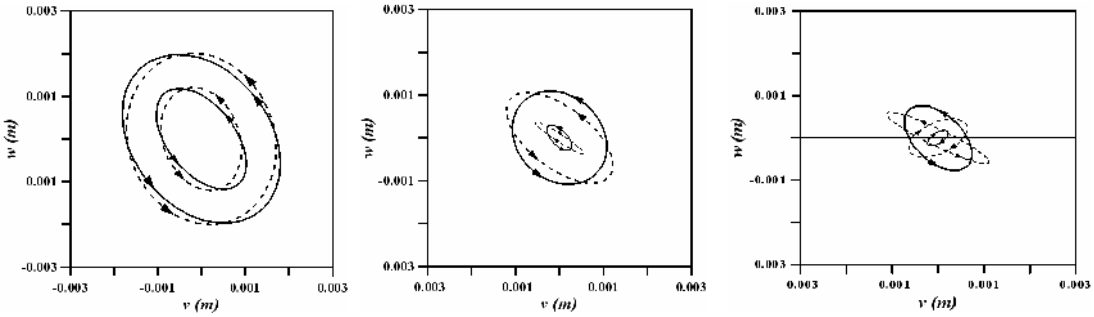

(a) $\Omega < \Omega_{cr1}$ (b) $\Omega_{cr1} < \Omega < \Omega_{cr2}$ (c) $\Omega_{cr2} < \Omega < \Omega_{cr3}$

Fig. 11. Whirling orbits at different rotational speed due to mutual effects of shaft misalignment and disk unbalance.

(35, 36) it is realized that the coupler stiffness affects the rotor's critical speeds and the offset acts like an excitation. As seen, resonance occurs at each critical speed and the FRF amplitude is proportional to the offset value.

Next, the whirling orbit and dynamic misalignment under different rotational speeds are investigated. The 10th (A) and the 11th (B) points are the front and the rear end of the misalignment. The parallel offset is set at $8.0 \times 10^{-4}\, m$. First, the orbits of two ends with K_L in rigid, sensitive, and soft area are shown in Figs. (8), (9) and (10), respectively. Three plots corresponding to (a) $\Omega < \Omega_{cr1}$ (b) $\Omega_{cr1} < \Omega < \Omega_{cr2}$ (c) $\Omega_{cr2} < \Omega < \Omega_{cr3}$ are shown. One can observe that the whirling orbit varies with the rotational speeds as expected. From Figs. 8 and 9, it is seen when the rotational speed $\Omega < \Omega_{cr1}$ and $\Omega_{cr1} < \Omega < \Omega_{cr2}$, both driving (A) and driven (B) ends are forward synchronous whirl, as shown in Figs. 8(a,b) and 9(a,b). At the rotational speed of $\Omega_{cr2} < \Omega < \Omega_{cr3}$, one sees that A becomes backward whirl but B remains forward whirl, as shown in Fig. 8(c) and Fig. 9(c). In Fig. 8, the dynamic offset basically retains the value e because of rigid K_L, but not in Fig. 9. When K_L falls in a soft area, both driving (A) and driven (B) ends show forward synchronous whirl at three regions, as shown in Fig. 10. The dynamic offset yet varies drastically with rotational speed due to soft coupler stiffness. As to the whirling orbits, it is a very complicated phenomenon. Usually as the rotation exceeds one critical speed, some parts of the rotor change their phase, i.e., from forward to backward or vice versa, but to precisely realize what parts change phase, a complete modal testing needs to be conducted. Figs. 8-10 show that the changing phenomena indeed do exist, serving as partial check of rotor behavior, but the authors have made no attempt to summarize any rule for this changing phenomenon.

Finally, the combined effects of shaft misalignment and disk unbalance are discussed. Fig. 11 shows the whirling orbits of the system with just misalignment (solid) and combined misalignment and unbalance (dash), with $e = 8.0 \times 10^{-4}\, m$, $r_e = 8.0 \times 10^{-4}\, m$. Three plots corresponding to (a) $\Omega < \Omega_{cr1}$ (b)

$\Omega_{cr1} < \Omega < \Omega_{cr2}$ (c) $\Omega_{cr2} < \Omega < \Omega_{cr3}$ are shown. From Fig. 11(a), it is seen that at lower rotation speed, shaft misalignment imposes more significant influence than the disk unbalance. The unbalance only slightly changes the orbit orientation. With the increase of rotational speeds, due to significant centrifugal force generated by disk unbalance, the orbits change in both orientation and magnitude.

4. Discussion and conclusions

The present research derived the transfer matrix for shaft coupler with parallel misalignment. The transfer matrices for rotating shaft, unbalanced disk, and oil-filmed bearing were derived in this paper as well for the integrity of TMM. The investigation reveals that coupler stiffness affects the critical speeds and the offset misalignment plays as an excitation. It is similar to the conclusion made by reference [15] that the misalignment hardly changed the rotor's critical speeds. During the derivation of a rotating shaft transfer matrix, the authors found that the boundary shears in two perpendicular directions were coupled together due to rotation. The coupling shears has the most effect as the shaft was free at both ends and it might drop the shaft's first critical speed up to 50%.

TMM derivation and numerical results in the present studies revealed that misalignment induced lateral response of the same frequency as rotational speed (1×) and that is unlike most of the researches where multiple integer (n×) components were found.

Though reference [17] obtained similar results to the present study, authors of that paper attributed the absence of 2× components to no consideration of non-linear effects of bearing and asymmetries of shafts. We, however, believe that the reason of n× components disappearing in our derivation is due to the coupler's torsional vibration not being considered. The coupler will transmit torque in addition to lateral and as long as the torsional flexibility of the coupler is taken into account the driven shaft will fluctuate in torsion such that it causes a non-constant rotation. The non-constant speed in conjunction with the misalignment and unbalance will consequently generate cyclic forces and moment effects on lateral vibration. It results in excitation of n× frequencies of the rotation speed as described in [13-15]. The authors are aware of the effect and are conducting the TMM for lateral and torsional vibration of a coupler.

Numerical results showed that the rotor's critical speeds varied with coupler's stiffness (K_L). Three regions associated with K_L were found. As K_L was soft the critical speeds depended mostly on the driving section, and as K_L was rigid the critical speeds depended on the whole set. As K_L was in between, the critical speeds became very sensitive to K_L. The whirling orbit across misalignment revealed that as rotational speed exceeded certain critical speeds the two ends of misalignment whirled asynchronously. The combined effects of disk unbalance and shaft misalignment showed that shaft misalignment imposed much greater effect than the disk unbalance at most rotational speeds. That means the shaft misalignment usually plays a dominating role. The effect of disk unbalance will become significant as the rotor runs at very high rotational speeds due centrifugal forces.

Nomenclature

A	:	The cross-section area
e	:	Static offset
l	:	The length of shaft
r	:	Dynamic offset
v, w	:	Displacements in Y and Z direction
I_{xx}	:	Polar moment of inertia
I_{yy} , I_{zz}	:	Transverse moment of inertia
K_B	:	Bending stiffness of the coupler
K_L	:	Linear stiffness of the coupler
M_Y, M_Z	:	Shaft's bending moments
V_Y, V_Z	:	Shaft's shear forces
$C_{yy}, C_{zz}, C_{yz}, C_{zy}$ $C_{\theta\theta}, C_{\phi\phi}, C_{\theta\phi}, C_{\phi\theta}$	:	Bearing's damping coefficients
$k_{yy}, k_{zz}, k_{yz}, k_{zy}$ $k_{\theta\theta}, k_{\phi\phi}, k_{\theta\phi}, k_{\phi\theta}$	:	Bearing's stiffness coefficients
$\{C\}$	:	Misalignment vector
$[G]$, $[\hat{G}]$	:	Shaft's left side transfer matrix
$[H]$, $[\hat{H}]$	:	Shaft's right side transfer matrix
$\{S\}^L$	:	Left side state vector
$\{S\}^R$	:	Right side state vector
$[T]_i$	:	Transfer matrix of *i-th* segment
$[T^u]$, $[T^m]$	:	Overall transfer matrix for unbalance and misalignment

$[T_s]$: Transfer matrix of a rotating shaft
$[T_d]$: Transfer matrix of an unbalanced disk
$[T_b]$: Transfer matrix of an oil-filmed bearing
$\{u_1\},\{u_2\}$: State vector of unbalance
ϕ, θ : Angular displacements
$\dot{\phi}, \dot{\theta}$: Angular velocity in Y and Z direction respectively
ρ : Density of shaft
δ_e : Deflection of the linear spring
γ_e : Phase relative to rotor's reference

References

[1] H. D. Nelson and J. M. McVaugh, The dynamics of rotor bearing systems using finite elements, *ASME Journal of Engineering for Industry*. 98 (1976) 593-600.

[2] H. N. özgüven, On the critical speed of continuous shaft-disk systems, *ASME Journal of Vibration, Acoustics, Stress, and Reliability in Design.*106 (1984) 59-61.

[3] H. N. özgüven and Z. L. özkan, Whirl speed and unbalance response of multi-bearing rotors using finite elements, *ASME Journal of Vibration, Acoustics, Stress, and Reliability in Design.* 106 (1984) 72-79.

[4] J. Gu, An improved transfer matrix-direct integration method for rotor dynamics, *ASME Journal of Vibration, Acoustics, Stress, and Reliability in Design.*108 **(**1986) 182-188.

[5] M. A. Prohl, A general method for critical speeds of flexible rotors, *Journal of Applied Mechanics.* 67 (1945) 142-148.

[6] J. W. Lund and F. K. Orcutt, Calculations and experiments on the unbalance response of a flexible rotor, *ASME Journal of Engineering for Industry.* 89 (1967) 785-796.

[7] J. W. Lund, Stability and damped critical speeds of flexible rotor in fluid-film bearings, *ASME Journal of Engineering for Industry*. 96 (1974) 509-516.

[8] S. W. Chao and S. C. Huang, On the flexural vibrations of shaft-disk systems using a modified transfer matrix method, *Proceedings of the 6th National Conference of the CSME*. Taipei, Taiwan. (1989) 1607-1618.

[9] N. F. Rieger and S. Zhou, Development and verification of transfer matrix unbalance response procedure for three-level rotor-foundation systems, *ASME Journal of Vibration and Acoustics* 120 **(**1**)** **(**1998) 240-251.

[10] J. W. Zu and Z. Ji, An improved transfer matrix method for steady-state analysis of nonlinear rotor bearing systems, *ASME Journal of Engineering for Gas Turbines and Power.* 124 (2) (2002) 303-310.

[11] B. B. Maharathi, P. R. Dash and A. K. Behera, Dynamic behaviour analysis of a dual-rotor system using the transfer matrix method, *International Journal of Acoustics and Vibration*s. 9 **(**3**)** **(**2004) 115-128.

[12] D. L. Dewell and L. D. Mitchell, Detection of a misaligned disk coupling using spectrum analysis, *ASME Journal of Vibration, Acoustics, Stress, and Reliability in Design.* 106 **(**1984) 9-16.

[13] M. Xu and R. D. Marangoni, Vibration analysis of a motor-flexible coupling-rotor ystem subject to misalignment and unbalance, Part Ⅰ: Theoretical model and Analysis, *Journal of Sound and Vibration.* 185 (4) (1994) 663-679.

[14] M. Xu and R. D. Marangoni, Vibration analysis of a motor-flexible coupling-rotor system subject to misalignment and unbalance, Part II: Experimental Validation, *Journal of Sound and Vibration.* 176 (5) (1994) 681-691.

[15] A. S. Sekhar and B. S. Prabhu, Effects of coupling misalignment on vibrations of rotating machinery, *Journal of Sound and Vibration*. 185 (4) (1995) 655-671.

[16] Y. S. Lee and C. W Lee, Modeling and vibration analysis of misaligned rotor-bearing system, *Journal of Sound and Vibration*. 224 (1) (1999) 17-32.

[17] K. M. Al-Hussain and I. Redmond, Dynamic response of two rotors connected by rigid mechanical coupling with parallel misalignment, *Journal of Sound and Vibration.* 249 (3) (2002) 483-498.

[18] K. M. Al-Hussain, Dynamic stability of two rigid rotors connected by flexible coupling with angular misalignment, *Journal of Sound and Vibration.* 266 (2003) 217-234.

[19] J. S. Rao, *Rotor Dynamics*, Wiley Eastern Limited, (1983).

Appendix

$$[T_s]_{8\times8}=[H]_{8\times8}[G]^{-1}_{8\times8},\ [\hat{T}_s]=[\hat{H}]\,[\hat{G}]^{-1} \tag{A1}$$

$$[H]_{8\times8}=\begin{bmatrix} H_{1,1} & H_{1,2} & H_{1,3} & H_{1,4} & 0 & 0 & 0 & 0 \\ H_{2,1} & H_{2,2} & H_{2,3} & H_{2,4} & 0 & 0 & 0 & 0 \\ H_{3,1} & H_{3,2} & H_{3,3} & H_{3,4} & 0 & 0 & 0 & 0 \\ H_{4,1} & H_{4,2} & H_{4,3} & H_{4,4} & H_{4,5} & H_{4,6} & H_{4,7} & H_{4,8} \\ 0 & 0 & 0 & 0 & H_{5,5} & H_{5,6} & H_{5,7} & H_{5,8} \\ 0 & 0 & 0 & 0 & H_{6,5} & H_{6,6} & H_{6,7} & H_{6,8} \\ 0 & 0 & 0 & 0 & H_{7,5} & H_{7,6} & H_{7,7} & H_{7,8} \\ H_{8,1} & H_{8,2} & H_{8,3} & H_{8,4} & H_{8,5} & H_{8,6} & H_{8,7} & H_{8,8} \end{bmatrix}$$

$$\begin{aligned}
&H_{1,1}=\cosh\lambda_1\ ;\ H_{1,2}=\sinh\lambda_1\ ;\ H_{1,3}=\cos\lambda_2\\
&H_{1,4}=\sin\lambda_2\\
&H_{2,1}=\beta_1\sinh\lambda_1\ ;\ H_{2,2}=\beta_1\cosh\lambda_1\\
&H_{2,3}=-\beta_2\sin\lambda_2\ ;\ H_{2,4}=\beta_2\cos\lambda_2\\
&H_{3,1}=EI_{zz}\beta_1^2\cosh\lambda_1\ ;\ H_{3,2}=EI_{zz}\beta_1^2\sinh\lambda_1\\
&H_{3,3}=EI_{zz}\beta_1^2\sinh\lambda_1\ ;\ H_{3,4}=EI_{zz}\beta_2^2\sin\lambda_2\\
&H_{4,1}=-\left[EI_{zz}\beta_1^3+\rho(I_{zz}\omega^2+I_{yy}\Omega^2)\beta_1\right]\sinh\lambda_1\\
&H_{4,2}=-\left[EI_{zz}\beta_1^3+\rho(I_{zz}\omega^2+I_{yy}\Omega^2)\beta_1\right]\cosh\lambda_1\\
&H_{4,3}=-\left[EI_{zz}\beta_2^3-\rho(I_{zz}\omega^2+I_{yy}\Omega^2)\beta_2\right]\sin\lambda_2\\
&H_{4,4}=\ \left[EI_{zz}\beta_2^3-\rho(I_{zz}\omega^2+I_{yy}\Omega^2)\beta_2\right]\cos\lambda_2\\
&H_{4,5}=\rho\Omega\omega(I_{yy}+I_{zz})\beta_3\sinh\lambda_3\\
&H_{4,6}=\rho\Omega\omega(I_{yy}+I_{zz})\beta_3\cosh\lambda_3\\
&H_{4,7}=-\rho\Omega\omega(I_{yy}+I_{zz})\beta_4\sin\lambda_4\\
&H_{4,8}=\rho\Omega\omega(I_{yy}+I_{zz})\beta_4\cos\lambda_4\\
&H_{5,5}=\cosh\lambda_3\ ;\ H_{5,6}=\sinh\lambda_3\ ;\ H_{5,7}=\cos\lambda_4\\
&H_{5,8}=\sin\lambda_4;H_{6,5}=-\beta_3\sinh\lambda_3\\
&H_{6,6}=-\beta_3\cosh\lambda_3\ ;\ H_{6,7}=\beta_4\sin\lambda_4\\
&H_{6,8}=-\beta_4\cos\lambda_4;H_{7,5}=-EI_{yy}\beta_3^2\cosh\lambda_3\\
&H_{7,6}=-EI_{yy}\beta_3^2\sinh\lambda_3\ ;\ H_{7,7}=EI_{yy}\beta_4^2\cos\lambda_4\\
&H_{7,8}=EI_{yy}\beta_4^2\sin\lambda_4\\
&H_{8,1}=\rho\Omega\omega(I_{yy}+I_{zz})\beta_1\sinh\lambda_1\\
&H_{8,2}=\rho\Omega\omega(I_{yy}+I_{zz})\beta_1\cosh\lambda_1\\
&H_{8,3}=-\rho\Omega\omega(I_{yy}+I_{zz})\beta_2\sin\lambda_2\\
&H_{8,4}=\rho\Omega\omega(I_{yy}+I_{zz})\beta_2\cos\lambda_2\\
&H_{8,5}=-\left[EI_{yy}\beta_3^3+\rho(I_{yy}\omega^2+I_{zz}\Omega^2)\beta_3\right]\sinh\lambda_3\\
&H_{8,6}=-\left[EI_{yy}\beta_3^3+\rho(I_{yy}\omega^2+I_{zz}\Omega^2)\beta_3\right]\cosh\lambda_3\\
&H_{8,7}=-\left[EI_{yy}\beta_4^3-\rho(I_{yy}\omega^2+I_{zz}\Omega^2)\beta_4\right]\sin\lambda_4\\
&H_{8,8}=\ \left[EI_{yy}\beta_4^3-\rho(I_{yy}\omega^2+I_{zz}\Omega^2)\beta_4\right]\cos\lambda_4
\end{aligned} \tag{A2}$$

$$[G]_{8\times8}=\begin{bmatrix} 1 & 0 & 1 & 0 & 0 & 0 & 0 & 0 \\ 0 & \beta_1 & 0 & \beta_2 & 0 & 0 & 0 & 0 \\ G_{3,1} & 0 & G_{3,3} & 0 & 0 & 0 & 0 & 0 \\ 0 & G_{4,2} & 0 & G_{4,4} & 0 & G_{4,6} & 0 & G_{4,8} \\ 0 & 0 & 0 & 0 & 1 & 0 & 1 & 0 \\ 0 & 0 & 0 & 0 & 0 & -\beta_3 & 0 & -\beta_4 \\ 0 & 0 & 0 & 0 & G_{7,5} & 0 & G_{7,7} & 0 \\ 0 & G_{8,2} & 0 & G_{8,4} & 0 & G_{8,6} & 0 & G_{8,8} \end{bmatrix} \tag{A3}$$

$$\lambda_1=l\beta_1,\ \lambda_2=l\beta_2,\ \lambda_3=l\beta_3,\ \lambda_4=l\beta_4$$

where elements of $[\hat{G}]$ and $[\hat{H}]$ are derivatives of $[G]$ and $[H]$, differences among them are

$$\begin{cases} \hat{G}_{4,6}=-G_{4,6} \\ \hat{G}_{4,8}=-G_{4,8} \\ \hat{G}_{8,2}=-G_{8,2} \\ \hat{G}_{8,4}=-G_{8,4} \end{cases} \begin{cases} \hat{H}_{4,5}=-H_{4,5} \\ \hat{H}_{4,6}=-H_{4,6} \\ \hat{H}_{4,7}=-H_{4,7} \\ \hat{H}_{4,8}=-H_{4,8} \end{cases} \begin{cases} \hat{H}_{8,1}=-H_{8,1} \\ \hat{H}_{8,2}=-H_{8,2} \\ \hat{H}_{8,3}=-H_{8,3} \\ \hat{H}_{8,4}=-H_{8,4} \end{cases} \tag{A4}$$

$$\begin{aligned}
&G_{3,1}=EI_{zz}\beta_1^2;\ G_{3,3}=-EI_{zz}\beta_2^2\\
&G_{4,2}=-EI_{zz}\beta_1^3-\rho(I_{zz}\omega^2+I_{zz}\Omega^2)\beta_1\\
&G_{4,4}=EI_{zz}\beta_2^3-\rho(I_{zz}\omega^2+I_{yy}\Omega^2)\beta_2
\end{aligned} \tag{A5}$$

$$\begin{aligned}
&G_{4,6}=\rho\Omega\omega(I_{yy}+I_{zz})\beta_3\\
&G_{4,8}=\rho\Omega\omega(I_{yy}+I_{zz})\beta_4\\
&G_{7,5}=-EI_{yy}\beta_3^2\ ;\ G_{7,7}=EI_{yy}\beta_4^2\\
&G_{8,2}=\rho\Omega\omega(I_{yy}+I_{zz})\beta_1\\
&G_{8,4}=\rho\Omega\omega(I_{yy}+I_{zz})\beta_2\\
&G_{8,6}=-EI_{yy}\beta_3^3-\rho(I_{yy}\omega^2+I_{zz}\Omega^2)\beta_3\\
&G_{8,8}=EI_{yy}\beta_4^3-\rho(I_{yy}\omega^2+I_{zz}\Omega^2)
\end{aligned} \tag{A6}$$

$$[T_d]=\begin{bmatrix} 1 & 0 & 0 & 0 & 0 & 0 & 0 & 0 \\ 0 & 1 & 0 & 0 & 0 & 0 & 0 & 0 \\ 0 & -I_z\omega^2 & 1 & 0 & 0 & -I_x\omega\Omega & 0 & 0 \\ -m\omega^2 & 0 & 0 & 1 & 0 & 0 & 0 & 0 \\ 0 & 0 & 0 & 0 & 1 & 0 & 0 & 0 \\ 0 & 0 & 0 & 0 & 0 & 1 & 0 & 0 \\ 0 & -I_x\omega\Omega & 0 & 0 & 0 & -I_x\omega^2 & 1 & 0 \\ 0 & 0 & 0 & 0 & -m\omega^2 & 0 & 0 & 1 \end{bmatrix}$$

$$[T_{b1}]=\begin{bmatrix} 1 & 0 & 0 & 0 & 0 & 0 & 0 & 0 \\ 0 & 1 & 0 & 0 & 0 & 0 & 0 & 0 \\ 0 & k_{\phi\phi} & 1 & 0 & 0 & C_{\phi\theta}\omega & 0 & 0 \\ k_{yy} & 0 & 0 & 1 & C_{yz}\omega & 0 & 0 & 0 \\ 0 & 0 & 0 & 0 & 1 & 0 & 0 & 0 \\ 0 & 0 & 0 & 0 & 0 & 1 & 0 & 0 \\ 0 & -C_{\theta\phi}\omega & 0 & 0 & 0 & k_{\theta\theta} & 1 & 0 \\ -C_{zy}\omega & 0 & 0 & 0 & k_{zz} & 0 & 0 & 1 \end{bmatrix}$$

$$[T_{b2}]=\begin{bmatrix} 0 & 0 & 0 & 0 & 0 & 0 & 0 & 0 \\ 0 & 0 & 0 & 0 & 0 & 0 & 0 & 0 \\ 0 & C_{\phi\phi}\omega & 0 & 0 & 0 & k_{\phi\theta} & 0 & 0 \\ C_{yy}\omega & 0 & 0 & 0 & k_{yz} & 0 & 0 & 0 \\ 0 & 0 & 0 & 0 & 1 & 0 & 0 & 0 \\ 0 & 0 & 0 & 0 & 0 & 1 & 0 & 0 \\ 0 & k_{\theta\phi} & 0 & 0 & 0 & -C_{\theta\theta}\omega & 0 & 0 \\ k_{zy} & 0 & 0 & 0 & -C_{zz}\omega & 0 & 0 & 0 \end{bmatrix}$$

$$[T_{b3}]_{ij}=-[T_{b2}]_{ij} \ ,besides \ [T_{b3}]_{3,2}=-[T_{b3}]_{3,2}$$
$$[T_{b3}]_{4,1}=-[T_{b3}]_{4,1}, [T_{b3}]_{7,6}=-[T_{b3}]_{7,6}$$
$$[T_{b3}]_{8,5}=-[T_{b3}]_{8,5}$$

(A13)

$$[T_{b4}]_{ij}=-[T_{b1}]_{ij} \ ,besides \ [T_{b4}]_{3,6}=-[T_{b1}]_{3,6}$$
$$[T_{b4}]_{4,5}=-[T_{b1}]_{4,5}, [T_{b4}]_{6,2}=-[T_{b1}]_{6,2}$$
$$[T_{b4}]_{7,1}=-[T_{b1}]_{7,1}$$

(A7)

$$[M_1]_{ij}=[M_4]_{ij}$$

$$=\begin{cases} 1 & ,when \ i=j \ , \ i=1\cdots8 \ , \ j=1\cdots8 \\ -1/k_B & ,when \ (i=2,j=3) \ and \ (i=6,j=7) \\ -1/k_L & ,when \ (i=1,j=4) \ and \ (i=5,j=8) \\ 0 & ,otherwise \end{cases}$$

$$[M_2]_{ij}=[M_3]_{ij}$$

$$=\begin{cases} 0 & ,when \ i\neq6 \ and \ j\neq3, i=1\cdots8 \ , \ j=1\cdots8 \\ -1/k_B & ,when \ i=6 \ and \ j=3, i=1\cdots8 \ , \ j=1\cdots8 \end{cases}$$

(A8)

Shyh-Chin Huang received a M.S. degree in Mechanical Engineering from University of Iowa in 1984, and a Ph.D. degree in Mechanical Engineering from Purdue University in 1987. Dr. Huang is currently a distinguished professor and researcher at National Taiwan University of Science and Technology. His research interests are in the area of vibration controls, smart materials and electric shunt damping design. Dr. Huang is currently an editor of Research Letters in Materials Science.

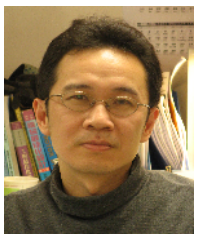

Chao-Yang Tsai received a M.S. degree in Mechanical Engineering from National Taiwan University of Science and Technology in 1997.Now he is studying at the same department for the Doctor Program. He is currently an instructor at the Army Academy R.O.C, teaching basic technological science including Engineering Mechanics, Mechanics Materials and so on.